

Parametric resonances of an electrically actuated piezoelectric nanobeam resonator considering surface effects and intermolecular interactions

S. Mehrdad Pourkiaee · Siamak E. Khadem · Majid Shahgholi

Received: 3 June 2015 / Accepted: 9 January 2016 / Published online: 25 January 2016
© Springer Science+Business Media Dordrecht 2016

Abstract This paper investigates the nonlinear dynamics of a parametrically excited doubly clamped piezoelectric nanobeam, actuated by a combined AC and DC loadings. Surface effects, intermolecular van der Waals forces, and fringing effects are incorporated in the nonlinear model. The governing equation of motion is obtained using the extended Hamilton principle. The reduced-order model equation (ROM) is obtained based on the Galerkin method. The multiple-scale method is applied directly to the nonlinear equation of motion and associated boundary conditions to obtain the nanobeam response analytically under small AC voltage loads. The influence of van der Waals forces, piezoelectric voltages, and surface effects is investigated on the natural frequencies, static equilibria, pull-in voltages, and principle parametric resonance (subharmonic resonance of order one-half) of the nanoresonator. It is shown the surface effect profoundly affects the nontrivial parametric responses, trivial stability zones, and bifurcation point's loci, and it is necessary to consider the surface effects for accurate and

exact investigation of the system response. The effect of piezoelectric voltage to control the dynamic instability region is also demonstrated. To validate analytical results, ROM equation is integrated numerically. It is seen that the perturbation results are in accordance with numerical results.

Keywords Nonlinear dynamics · Parametric resonance · Perturbation method · Surface effects · Intermolecular forces · Clamped–clamped piezoelectric nanobeam

1 Introduction

In recent years, nanoelectromechanical systems (NEMSs) have been the focus of attention of vast majority of researchers. Thanks to their inherent characteristics, NEMSs are being used in wide variety of applications such as capacitive sensors, actuators, narrow band filtering, mass and force detection, and atomic force microscopes. NEMS resonators excited electrostatically and could experience different sources of nonlinearity such as molecular interactions (Casimir and van der Waals forces) and nonlinear electrostatic forces. This reveals the importance of the nonlinear dynamics in modeling a NEMS-based resonator under electrostatic actuation. Parametric resonance, as a nonlinear phenomenon, has received great attentions in practice and the literature for its peculiar effects, such as low sensitivity to damping, sharp transition

S. M. Pourkiaee · S. E. Khadem (✉)
Department of Mechanical Engineering, Tarbiat Modares University, P.O. Box 14115-177, Tehran, Iran
e-mail: Khadem@modares.ac.ir

S. M. Pourkiaee
e-mail: M.Pourkiaee@modares.ac.ir

M. Shahgholi
Department of Mechanical Engineering, Shahid Rajaei Teacher Training University, Tehran, Iran
e-mail: Majid.Shahgholi@srttu.edu

between zero and nonzero responses, large resonant responses, and hence, higher signal-to-noise ratios. Compared to the conventional excitation techniques, parametric excitations occur in the systems with time-dependent (periodic) parameters. Many studies have been carried out in the literature on the nonlinear behavior of the NEMS/MEMS resonators. Carunta and Martinez [1] studied the parametric resonance of a MEMS cantilever. Damping, voltage, and fringing effects on the parametric response were reported. Rhoads et al. [2] explored the nonlinear dynamics of an electromagnetically actuated microcantilever under parametric excitations. The fifth-order nonlinearity was investigated using the perturbation methods. Abdel-Rahman and Nayfeh [3] investigated secondary resonances of electrically actuated resonant microsensors analytically using the method of the multiple scales. Nonlinear dynamics of NEMS-based sensors under superharmonic resonance was investigated by Kacem et al. [4] using the method of multiple scales. They obtained a way to retard the pull-in voltage by decreasing the AC voltage. Ouakad and Younis [5] studied nonlinear dynamics of an electrostatically actuated carbon nanotube (CNT) resonator. Primary and secondary resonances were studied using shooting method [6, 7]. Several nonlinear phenomena have been reported such as hysteresis [8, 9], dynamic pull-in [10–12], hardening behavior [11, 13], and softening behavior [14]. In a series of work [15–18], they investigated the nonlinear dynamics of a CNT resonator in the presence of the initial curvature. They studied the effect of DC electrostatic force and the slack level on the CNT natural frequencies and mode shapes. In Ref. [18], they provided a model to study the forced vibration response of the CNTs under small DC and AC loads using the perturbation techniques. Rasekh and Khadem [19] investigated pull-in instability of a CNT cantilever using direct numerical integration. Curvature and inertia nonlinearities were also taken into account. Hajnayeb and Khadem [20, 21] investigated in depth the stability and the nonlinear vibrations of single-walled and double-walled CNTs under electrostatic actuations. Primary and secondary resonances and bifurcation points under different values of DC and AC voltages were studied using the multiple-scale method. Nonlinear van der Waals forces acting between the CNT and the ground plane, due to the small gap, have been studied in Ref. [20]. Ouakad et al. [22], studied both static and dynamic behaviors of a clamped–clamped CNT resonator using

a novel discretization technique: differential quadrature method and finite difference method (DQM–FDM). Different phenomena such as dynamic pull-in and frequency veering were studied. Alibeigloo and Emtehani [23] performed a study on static and free vibration behavior of carbon nanotube-reinforced composite (CNTRC) using DQM. Xu and Younis [24] investigated the nonlinear dynamics of a CNT actuated under large electrostatic forces. They expanded the nonlinear electrostatic term into enough number of terms of the Taylor series. Also, many studies in the literature have focused on the piezoelectric actuation, one of the common sources of excitation of the NEMS-based resonators. Asemi et al. [25] obtained a nonlinear continuum model for the large-amplitude vibration of nanoelectromechanical resonators using piezoelectric nanofilms (PNFs) under external electric voltage. Alibeigloo and Liew [26] studied bending and free vibration of a functionally graded CNTRC beam, embedded in piezoelectric layers using the DQM. Both the direct and inverse piezoelectric effects were investigated. Ke et al. [27] investigated the nonlinear vibration of the piezoelectric nanobeams based on the nonlocal and Timoshenko beam theory using the DQM. They studied the effect of nonlocal parameter and piezoelectric voltage on the nanobeam behavior. Arani et al [28] performed a study on the nonlinear dynamic stability of single-layered graphene sheets (SLGSs) integrated with zinc oxide (ZnO) actuators and sensors using the differential cubature method. They showed that magnetic field and the external voltage are affecting parameters to control the dynamic instability region. According to the literature, almost every performed research, studying the parametric resonance of the electromechanical systems, is microsized problems. Furthermore, in most of the valuable studies performed to analyze nonlinear dynamics of NEMS resonators, the size-dependent properties have been neglected, and there is no clear distinction between those and microsized problems. It is beneficial to mention that reducing size to nanoscales leads to size-dependent behaviors of nanostructures [29, 30]. Moreover, large surface area-to-volume ratio is an important consequence of the scale down. Large surface-to-bulk ratio at nanoscales results in an increase in the surface energy [31]. Therefore, surface energies could remarkably affect the static and the dynamic behaviors of nanoscaled structures. Many studies have been carried out by researchers to investigate the influence of the surface effects on nanostructures. Wang

and Wang [32] studied the effect of surface energy on free vibration of a cracked nanobeam. They showed that the natural frequencies of the nanobeam have dramatic dependence on surface stresses. Eltahir et al. [33] investigated the coupling effects of nonlocal and surface energy on vibration of nanobeams using Galerkin finite element technique. There are also numerous papers in the literature which have reported the influence of surface energy on pull-in instability [34–36], buckling [37, 38], and free vibration [39] of nanostructures. It can be found that, based on the literature, there are few articles in which dynamic analysis at nanoscales considering the surface stresses have been presented. Also, there is still lacking of strong theoretical model in the literature which illustrates the surface effects on the dynamic behavior of the nanoresonators. Accordingly, it seems that studying principle parametric resonances of an electrostatically actuated piezoelectric nanobeam gives out interesting results. This study attempts to provide a realistic model to demonstrate the static and dynamic responses of a piezoelectric nanoresonator and the physical behaviors peculiar to the nanosized systems. To this end, surface effects and intermolecular van der Waals forces are taken into account, due to the size effect at the nanoscale and the small initial gap between the electrodes. Furthermore, in-depth study of the nonlinear parametric resonances of the nanobeam under small AC loads is presented using the multiple-scale method. The effect of different physical parameters on static pull-in, frequency–response curves, and bifurcation points is investigated. Numerical simulation is performed to validate perturbation solutions.

2 Problem formulation

Figure 1 depicts the considered piezoelectric nanoresonator and the xyz inertial coordinate system which passes through the centroid of the cross section ($y = 0, z = 0$) and is located at the left clamped end of the nanobeam. The vertical displacement of the nanobeam centerline along the z -axis is denoted by $w(x, t)$.

The movable nanobeam is of length L , width b , and thickness h and is surrounded between two conductive electrodes of different lengths. The piezoelectric nanobeam is actuated by the electric load $V_{DC} + V_{AC} \cos(\Omega t)$ through the lower electrode and the V_{DC} load through the upper electrode where V_{DC} is the DC

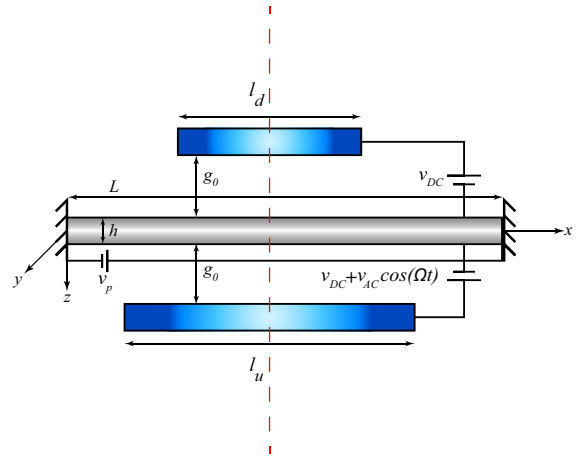


Fig. 1 Schematic diagram of an electrically actuated clamped–clamped piezoelectric nanobeam

bias voltage, and V_{AC} and Ω are the amplitude and frequency of the AC voltage, respectively. In addition, the piezoelectric nanobeam is actuated by the direct current polarization voltage V_P , which is applied through the thin electrodes at the nanobeam ends (the realistic devices based on the current model are discussed in Refs. [40, 41]). The initial capacitor gap width g_0 is assumed to be under 20 nm, such that the van der Waals force becomes dominant as an intermolecular interaction between the electrodes [42]. Van der Waals force is given by:

$$F_{vdW} = \frac{A_h b}{6\pi (g_0 - w(x, t))^3} H_1(x) - \frac{A_h b}{6\pi (g_0 + w(x, t))^3} H_2(x) \tag{1}$$

$$H_1(x) = H\left(x - \frac{L - l_u}{2}\right) - H\left(x - \frac{L + l_u}{2}\right) \tag{2}$$

$$H_2(x) = H\left(x - \frac{L - l_d}{2}\right) - H\left(x - \frac{L + l_d}{2}\right) \tag{3}$$

where A_h is the Hamker constant with values in the range of $[0.4 - 4] \times 10^{-19} \text{ J}$ [43], and $H(x)$ is the Heaviside function indicating the van der Waals force distribution. The electrostatic force can be expressed as:

$$F_{es} = \frac{1}{2} \varepsilon_0 \frac{b C_n [(V_{DC} - V_P) + V_{AC} \cos(\Omega t)]^2}{(g_0 - w(x, t))^2} H_1(x) - \frac{1}{2} \varepsilon_0 \frac{b C_n [V_{DC} - V_P]^2}{(g_0 + w(x, t))^2} H_2(x) \tag{4}$$

where ε_0 is the permittivity of the gap medium, and $C_n = 1 + 1.9861 (g_0/b)^{0.8258}$ is due to the fringing

field effect [8]. It is worthy to note that the initial gap is comparable to the nanobeam width; consequently, the fringing field effect is considered.

2.1 Surface energy

To incorporate the surface effects, the Gurtin–Murdoch surface elasticity model is utilized. It is assumed that the elastic surface has a mathematically zero thickness which is perfectly bonded to the bulk material, and there is no slipping between the bulk and the surface. According to the surface elasticity theory, surface stresses in the $x - z$ plane can be expressed as [44,45]:

$$\tau_{xx} = \tau_0 + E^s \varepsilon_x \tag{5}$$

$$\tau_{xz} = \tau_0 \frac{\partial w(x, t)}{\partial x} \tag{6}$$

where τ_0 and E^s are surface residual stress and surface elastic modulus, respectively. It is noted that the unit of the surface stresses (i.e., τ_0 , τ_{xx} , τ_{xz}) and the surface elastic modulus (E^s) in the SI system is N/m. In Eq. (5), ε_x represents the nonlinear strain in the beam axial direction, given by:

$$\varepsilon_x = \frac{\partial u_0(x, t)}{\partial x} - z \frac{\partial^2 w(x, t)}{\partial x^2} + \frac{1}{2} \left(\frac{\partial w(x, t)}{\partial x} \right)^2 \tag{7}$$

where $u_0(x, t)$ denotes the axial displacement along the x -axis. The surface strain energy in the deformed surface area is given by:

$$U_S = \int_{\bar{A}} \gamma d\bar{A}, \gamma = \tau_0 + \frac{1}{2} E^s \varepsilon_x^2 + \frac{1}{2} \tau_{xz} \varepsilon_{xz} \tag{8}$$

where \bar{A} is the surface area of the nanobeam, and γ is the strain energy density of the surface. Note that the unit of the strain energy density (γ), in the SI system, is N/m, and all the terms are compatible according to dimension unit. For a differential element of the surface layer, it can be written as:

$$d\bar{A} = dA_S ds \tag{9}$$

where dA_S is the differential perimeter element, and ds is the length of the deformed element, given by:

$$ds = \sqrt{(1 + u_0')^2 + (w')^2} dx \approx \left(1 + u_0' + \frac{w'^2}{2} \right) dx \tag{10}$$

where the prime denotes derivative with respect to x . Introducing Eqs. (9) and (10) into Eq. (8), the surface energy can be found in the form of:

$$U_S = \int_0^L \oint_{\partial A_S} \left(\tau_0 + \frac{E^s}{2} \left(u_0' + \frac{w'^2}{2} - zw'' \right)^2 + \frac{1}{2} \tau_0 (w')^2 \right) \left(1 + u_0' + \frac{w'^2}{2} \right) dA_S dx \tag{11}$$

Noting that τ_{xx} is distributed along the entire perimeter of cross section, and τ_{xz} is acting along the top and bottom surfaces, the surface elastic energy up to the second-order products yields to:

$$U_S = \tau_0 A^s \int_0^L \left(1 + u_0' + \frac{w'^2}{2} \right) dx + \frac{E^s I^s}{2} \int_0^L (w'')^2 dx + \frac{E^s A^s}{2} \int_0^L \left(u_0' + \frac{w'^2}{2} \right)^2 dx + \tau_0 \bar{A}^s \int_0^L \frac{(w')^2}{2} dx \tag{12}$$

where $I^s = \oint_{\partial A_S} z^2 dA_S = (bh^2/2 + h^3/6)$ is the perimeter moment of inertia of the beam cross section about the y -axis, $A^s = 2(b + h)$ is the perimeter of the cross section, and $\bar{A}^s = 2b$. Note that, here, the surface energy of the nanobeam is obtained by neglecting the piezoelectricity effects of the surface due to the lack of strong and comprehensive theoretical model in the literature.

2.2 Bulk energy

Piezoelectric materials are able to convert the applied electrical potential load into mechanical displacements (converse piezoelectric effect). To consider the electro-mechanical behavior of the piezoelectric nanobeam, it is assumed that the electric potential variation between the top and the bottom surface layers is equal to V_p , and the piezoelectric nanobeam is polarized along the z -direction; hence, the one-dimensional constitutive law for the considered piezoelectric nanobeam can be expressed as [46–48]:

$$\begin{aligned} \sigma_x &= E \varepsilon_x - \bar{e}_{31} E_z \\ D_z &= \bar{e}_{31} \varepsilon_x + \lambda_{33} E_z \end{aligned} \tag{13}$$

where E is the Young’s modulus of the bulk (with the unit N/m^2), $E_z = V_p/h$ is the one-dimensional electrical field vector, D_z is the one-dimensional electric displacement, \bar{e}_{31} and λ_{33} are transversal piezoelectric coefficient and permittivity constant, respectively. The surface equilibrium relations are given by:

$$\begin{aligned} \tau_{\beta i, \beta}^+ - \sigma_{iz}^+ &= \rho^s a_i^+ \\ \tau_{\beta i, \beta}^- + \sigma_{iz}^- &= \rho^s a_i^- \end{aligned} \tag{14}$$

where $(\cdot)_{,x}$ represents the derivative with respect to β , and “ \pm ” denotes the upper and the bottom surfaces, respectively. ρ^s is the mass density of surface layer, $\tau_{\beta i}$ is the surface stress, and σ_{iz} is the surface force per unit area (bulk stress). In Eq. (14), $\beta = x, y$ and $i = x, y, z$. Equation (14) first was introduced in the literature by Gurtin and Murdoch. In the classical beam theories, bulk stress σ_z is assumed to be zero. This assumption violates the surface equilibrium, Eq. (14). To satisfy equilibrium conditions on the surface layer, this assumption is ignored. According to [49], it is assumed that σ_z varies linearly through the thickness of the nanobeam as follows:

$$\sigma_z = \frac{1}{2} (\sigma_z^+ + \sigma_z^-) + \frac{1}{h} (\sigma_z^+ - \sigma_z^-) z \tag{15}$$

where σ_z^+ and σ_z^- are the stresses at the top and the bottom layers, respectively. Substituting Eq. (15) into Eq. (14), and noticing that the top and the bottom displacements are identical, gives:

$$\sigma_z = \frac{2z}{h} \left(\tau_0 \frac{\partial^2 w(x, t)}{\partial x^2} - \rho^s \frac{\partial^2 w(x, t)}{\partial t^2} \right) \tag{16}$$

The total axial stress in the bulk material of the nanobeam is:

$$\sigma_x = E \varepsilon_x + \nu \sigma_z - \bar{e}_{31} E_z \tag{17}$$

where ν is the Poisson’s ratio of the nanobeam bulk material. The stored strain energy in the bulk material of the piezoelectric nanobeam can be obtained by [50]:

$$U_B = \frac{1}{2} \int_V \sigma_x \varepsilon_x dV - \frac{1}{2} \int_V D_z E_z dV \tag{18}$$

By substituting Eqs. (7), (13), and (17) into Eq. (18), one can obtain:

$$\begin{aligned} U_B &= \frac{EA}{2} \int_0^L \left(u_0' + \frac{w^2}{2} \right)^2 dx \\ &+ \frac{1}{2} \left(EI - \frac{2\nu I \tau_0}{h} \right) \int_0^L (w'')^2 dx \\ &+ \frac{\nu I \rho^s}{h} \int_0^L \ddot{w} w'' dx \\ &- \frac{V_p b \bar{e}_{31}}{2} \int_0^L (w')^2 dx \end{aligned} \tag{19}$$

where I denotes the area moment of inertia of the cross section of the nanobeam, A denotes the area of the cross section, and the dot denotes the derivative with respect to t .

2.3 Equation of motion

The total strain energy of the nanobeam which is composed of the strain energies of the bulk and of the surface layer can be found in the form of:

$$U = U_B + U_S \tag{20}$$

Similarly, the total kinetic energy of the nanobeam which is composed of the kinetic energies of the bulk and of the surface layer is defined as:

$$T = \frac{(\rho A + \rho^s A^s)}{2} \int_0^L \dot{w}^2 dx \tag{21}$$

The work done by the electrostatic and van der Waals forces is equal to:

$$W_{NC} = \int_0^L \int_0^w (F_{es} + F_{vdW}) dw dx \tag{22}$$

The governing equation of the motion is obtained by the extended Hamilton principle, which is defined as follows:

$$\int_{t_1}^{t_2} \delta H dt = \int_{t_1}^{t_2} \delta (T - U + W_{NC}) dt = 0 \tag{23}$$

Substituting Eqs. (20)–(22) into Eq. (23), and applying the variational approach and grouping the terms, the governing equation of motion is obtained as follows:

$$\begin{aligned}
 & (EI)_{\text{eff}} \frac{\partial^4 w(x, t)}{\partial x^4} + (\rho A)_{\text{eff}} \frac{\partial^2 w(x, t)}{\partial t^2} \\
 & + (\rho I)_{\text{eff}} \frac{\partial^4 w(x, t)}{\partial x^2 \partial t^2} - \left[F_S + F_P \right. \\
 & \left. + \frac{(EA)_{\text{eff}}}{2L} \int_0^L \left(\frac{\partial w(x, t)}{\partial x} \right)^2 dx \right] \frac{\partial^2 w(x, t)}{\partial x^2} \\
 & = \frac{1}{2} \varepsilon_0 \frac{bC_n (V_D + V_{AC} \cos(\Omega t))^2}{(g_0 - w(x, t))^2} H_1(x) \\
 & - \frac{1}{2} \varepsilon_0 \frac{bC_n V_D^2}{(g_0 + w(x, t))^2} H_2(x) \\
 & + \frac{A_h b}{6\pi (g - w(x, t))^3} H_1(x) \\
 & - \frac{A_h b}{6\pi (g + w(x, t))^3} H_2(x) \tag{24}
 \end{aligned}$$

where:

$$\begin{aligned}
 F &= F_{\text{es}} + F_{\text{vdW}}, \quad (EI)_{\text{eff}} = EI + E^s I^s \\
 & - \frac{2\nu I \tau_0}{h}, \quad (EA)_{\text{eff}} = EA + E^s A^s, \\
 (\rho A)_{\text{eff}} &= \rho A + \rho^s A^s, \quad (\rho I)_{\text{eff}} = \frac{2\nu I \rho^s}{h}, \\
 F_S &= \tau_0(4b + 2h), \quad F_P = -V_P b \bar{z}_{31}, \\
 V_D &= V_{DC} - V_P \tag{25}
 \end{aligned}$$

The nanobeam is clamped at both ends, and hence, the boundary conditions are:

$$w(0, t) = w(L, t) = 0, \quad \frac{\partial w(0, t)}{\partial x} = \frac{\partial w(L, t)}{\partial x} = 0 \tag{26}$$

For the sake of simplicity, the following dimensionless quantities are introduced:

$$w^* = \frac{w}{g_0}, \quad x^* = \frac{x}{L}, \quad t^* = \frac{t}{\tilde{t}}, \quad \Omega^* = \Omega \tilde{t} \tag{27}$$

where \tilde{t} (i.e., the characteristic time) is defined as:

$$\tilde{t} = \sqrt{\frac{(\rho A)_{\text{eff}} L^4}{(EI)_{\text{eff}}}} \tag{28}$$

Substituting Eq. (27) into Eqs. (25) and (26), dropping the stars for simplicity, the dimensionless equation of motion by considering viscous damping and the associated boundary conditions can be written as:

$$\begin{aligned}
 & \frac{\partial^4 w}{\partial x^4} + \frac{\partial^2 w}{\partial t^2} - [\alpha_1 + \alpha_2 + \alpha_3 \Gamma(w, w)] \frac{\partial^2 w}{\partial x^2} \\
 & + \alpha_4 \frac{\partial^4 w}{\partial x^2 \partial t^2} + \alpha_5 \frac{\partial w}{\partial t} \\
 & = \alpha_6 \frac{[V_D + V_{AC} \cos(\Omega t)]^2}{(1 - w)^2} H_1(x) \\
 & - \alpha_6 \frac{V_D^2}{(1 + w)^2} H_2(x) \\
 & + \alpha_7 \frac{H_1(x)}{(1 - w)^3} - \alpha_7 \frac{H_2(x)}{(1 + w)^3} \tag{29}
 \end{aligned}$$

$$w(0, t) = w(1, t) = 0, \quad \frac{\partial w(0, t)}{\partial x} = \frac{\partial w(1, t)}{\partial x} = 0 \tag{30}$$

The function Γ and the nondimensional parameters appearing in Eq. (29) are defined as:

$$\begin{aligned}
 \Gamma(f_1(x, t), f_2(x, t)) &= \int_0^1 \frac{\partial f_1}{\partial x} \cdot \frac{\partial f_2}{\partial x} dx, \\
 \alpha_1 &= \frac{F_P L^2}{(EI)_{\text{eff}}}, \quad \alpha_2 = \frac{F_S L^2}{(EI)_{\text{eff}}}, \quad \alpha_3 = \frac{(EA)_{\text{eff}} g_0}{2(EI)_{\text{eff}}}, \\
 \alpha_4 &= \frac{2\nu I \rho^s}{h L^2 (\rho A)_{\text{eff}}}, \quad \alpha_5 = \frac{c L^2}{\sqrt{(\rho A)_{\text{eff}} (EI)_{\text{eff}}}}, \\
 \alpha_6 &= \frac{1}{2} \frac{\varepsilon b C_n L^4}{g_0^3 (EI)_{\text{eff}}}, \quad \alpha_7 = \frac{\tilde{A} b L^4}{6\pi g_0^4 (EI)_{\text{eff}}}, \\
 H_1(x) &= H\left(x - \frac{L - l_u}{2L}\right) - H\left(x - \frac{L + l_u}{2L}\right), \\
 H_2(x) &= H\left(x - \frac{L - l_d}{2L}\right) - H\left(x - \frac{L + l_d}{2L}\right) \tag{31}
 \end{aligned}$$

3 The reduced-order model

To generate the reduced-order model of the system using the Galerkin discretization method, the nanobeam deflection is approximated as:

$$w(x, t) = \sum_{i=1}^n q_i(t) \varphi_i(x) \tag{32}$$

where $q_i(t)$ is the i th time-dependent generalized coordinate, and $\varphi_i(x)$ is the i th eigenfunction of the clamped-clamped linear undamped nanobeam, considering the surface effects and axial load due to piezoelectric actuation. Note here that $\varphi_i(x)$ is normalized such that $\int_0^1 \varphi_i \varphi_j dx = \delta_{ij}$ and satisfies the following eigenvalue problem:

$$\begin{aligned} \varphi_i^{IV} &= (\alpha_1 + \alpha_2)\varphi_i'' + \omega_{non,i}^2(\varphi_i + \alpha_4\varphi_i'') \\ \varphi_i(x) = 0\varphi_i'(x) = 0 & \text{ at } x = 0 \text{ and } x = 1 \end{aligned} \tag{33}$$

where $\omega_{non,i}$ is the i th dimensionless natural frequency of the nanobeam. To include complete contribution of the nonlinear electrostatic and van der Waals forces, Eq. (29) is multiplied by $\varphi_n (1 - w^2)^3$. Substituting Eq. (32) into the resulting equation and using Eq. (33) to eliminate φ_i^{IV} , and integrating the outcome from $x = 0$ to 1, would reduce it to nonlinear differential equations in terms of generalized coordinates, $q_i(t)$. According to [5, 8], it is sufficient to consider one mode to obtain the discretized equation of NEMS systems. One-mode approximation yields to:

$$\begin{aligned} & (\ddot{q}_1 + \alpha_5\dot{q}_1 + \omega_1^2q_1) \left(1 - 3q_1^2 \int_0^1 \varphi_1^4 dx \right. \\ & \quad \left. + 3q_1^4 \int_0^1 \varphi_1^6 dx - q_1^6 \int_0^1 \varphi_1^8 dx \right) \\ & \quad + (\ddot{q}_1 + \omega_1^2q) \left(\alpha_4 - 3\alpha_4q_1^2 \int_0^1 \varphi_1''\varphi_1^3 dx \right. \\ & \quad \left. + 3\alpha_4q_1^4 \int_0^1 \varphi_1''\varphi_1^5 dx - \alpha_4q_1^6 \int_0^1 \varphi_1''\varphi_1^7 dx \right) \\ & \quad - \alpha_3q_1^3\Gamma(\varphi_1, \varphi_1) \left(\int_0^1 \varphi_1''\varphi_1 dx - 3q_1^2 \int_0^1 \varphi_1''\varphi_1^3 dx \right. \\ & \quad \left. + 3q_1^4 \int_0^1 \varphi_1''\varphi_1^5 dx - q_1^6 \int_0^1 \varphi_1''\varphi_1^7 dx \right) \\ & = \alpha_6 (V_D + V_{AC} \cos(\Omega t))^2 \left(\int_{lba}^{uba} \varphi_1 dx \right. \\ & \quad \left. + 2q_1 \int_{lba}^{uba} \varphi_1^2 dx - 2q_1^3 \int_{lba}^{uba} \varphi_1^4 dx \right. \\ & \quad \left. - q_1^4 \int_{lba}^{uba} \varphi_1^5 dx \right) \\ & \quad - \alpha_6 V_D^2 \left(\int_{lbd}^{ubd} \varphi_1 dx - 2q_1 \int_{lbd}^{ubd} \varphi_1^2 dx \right. \\ & \quad \left. + 2q_1^3 \int_{lbd}^{ubd} \varphi_1^4 dx - q_1^4 \int_{lbd}^{ubd} \varphi_1^5 dx \right) \\ & \quad + \alpha_7 \left(\int_{lba}^{uba} \varphi_1 dx + 3q_1 \int_{lba}^{uba} \varphi_1^2 dx \right. \\ & \quad \left. + 3q_1^2 \int_{lba}^{uba} \varphi_1^3 dx + q_1^3 \int_{lba}^{uba} \varphi_1^4 dx \right) \\ & \quad - \alpha_7 \left(\int_{lbd}^{ubd} \varphi_1 dx - 3q_1 \int_{lbd}^{ubd} \varphi_1^2 dx \right. \\ & \quad \left. + 3q_1^2 \int_{lbd}^{ubd} \varphi_1^3 dx - q_1^3 \int_{lbd}^{ubd} \varphi_1^4 dx \right) \end{aligned} \tag{34}$$

where:

$$\begin{aligned} lba &= \frac{L - l_u}{2L}, \quad uba = \frac{L + l_u}{2L}, \quad lbd = \frac{L - l_d}{2L}, \\ ubd &= \frac{L + l_d}{2L} \end{aligned} \tag{35}$$

Eq. (34) can be numerically integrated using the Runge–Kutta technique to simulate the dynamic behavior of the nanobeam.

4 Static deflection and the corresponding natural frequencies

The nanobeam deflection under electrostatic excitation is composed of the dynamic component $u(x, t)$, due to the AC voltage and the static component $w_s(x)$, due to the DC voltage:

$$w(x, t) = w_s(x) + u(x, t) \tag{36}$$

To calculate the static deflection and boundary conditions, all time-varying terms in Eqs. (29) and (30) are set equal to zero, and the following results are obtained:

$$\begin{aligned} w_s^{IV}(x) - [\alpha_1 + \alpha_2 + \alpha_3\Gamma(w_s, w_s)] w_s'' & \\ = \alpha_6 \frac{V_D^2}{(1 - w_s)^2} H_1(x) - \alpha_6 \frac{V_D^2}{(1 + w_s)^2} H_2(x) & \\ + \alpha_7 \frac{H_1(x)}{(1 - w_s)^3} - \alpha_7 \frac{H_1(x)}{(1 + w_s)^3} & \end{aligned} \tag{37}$$

$$w_s(x = 0, 1) = 0 \text{ and } w_s'(x = 0, 1) = 0 \tag{38}$$

To calculate the static deflection, w_s can be expressed as:

$$w_s = \sum_{i=1}^M c_i \varphi_i^s \tag{39}$$

where φ_i^s is a comparison function, and c_i is an unknown constant coefficient which can be obtained using the Galerkin method. Substituting Eq. (39) in Eq. (37) and multiplying the resulting equations by φ_n^s , and integrating the outcome from $x = 0$ to 1, results in the system of M algebraic equations. The constant coefficients are then obtained by solving these equations. According to the [5], one-mode approximation is sufficient to obtain the static deflection. Substituting Eq. (36) in Eq. (29) and using Eq. (37) to eliminate the static equilibrium position, and expanding the electrostatic and dispersion forces around the stability point,

yields to equations governing the dynamic behavior of the nanobeam:

$$\begin{aligned} & \ddot{u} + \alpha_5 \dot{u} + u^{IV} - [\alpha_1 + \alpha_2 + \alpha_3 \Gamma(w_s, w_s)] u'' \\ & - 2\alpha_3 \Gamma(w_s, u) u - 2\alpha_3 \Gamma(w_s, u) w_s'' - \alpha_3 \Gamma(u, u) w_s'' \\ & - \alpha_3 \Gamma(u, u) u'' + \alpha_4 \ddot{u}'' \\ & = \alpha_{61} \left(\frac{2V_D^2}{(1-w_s)^3} u + \frac{3V_D^2}{(1-w_s)^4} u^2 + \frac{4V_D^2}{(1-w_s)^5} u^3 \right) \\ & - \alpha_{62} \left(\frac{-2V_D^2}{(1+w_s)^3} u + \frac{3V_D^2}{(1+w_s)^4} u^2 - \frac{4V_D^2}{(1+w_s)^5} u^3 \right) \\ & + \alpha_{71} \left(\frac{3}{(1-w_s)^4} u + \frac{6}{(1-w_s)^5} u^2 + \frac{10}{(1-w_s)^6} u^3 \right) \\ & - \alpha_{72} \left(\frac{-3}{(1+w_s)^4} u + \frac{6}{(1+w_s)^5} u^2 - \frac{10}{(1+w_s)^6} u^3 \right) \end{aligned} \tag{40}$$

According to [51], V_{AC}^2 is dropped due to the fact $V_{AC}^2 \ll V_D^2$. The linearized equation of the undamped free vibration of the double clamped nanobeam can be obtained by dropping the forcing, damping, and the nonlinear terms of Eq. (40) as follows:

$$\begin{aligned} & \ddot{u} + u^{IV} - [\alpha_1 + \alpha_2 + \alpha_3 \Gamma(w_s, w_s)] u'' \\ & - 2\alpha_3 \Gamma(w_s, u) w_s'' + \alpha_4 \ddot{u}'' \\ & = \alpha_{61} \frac{2V_D^2}{(1-w_s)^3} u + \alpha_{62} \frac{2V_D^2}{(1+w_s)^3} u \\ & + \alpha_{71} \frac{3}{(1-w_s)^4} u + \alpha_{72} \frac{3}{(1+w_s)^4} u \end{aligned} \tag{41}$$

The fundamental natural frequencies and the corresponding mode shapes can be obtained by solving the eigenvalue problem associated with Eq. (41). Letting $u = \phi_n(x) e^{i\omega_n t}$ reduces Eq. (41) to:

$$\begin{aligned} & \phi_n^{IV} - \omega_n^2 \phi_n + \alpha_4 \omega_n^2 \phi_n'' - [\alpha_1 + \alpha_2 + \alpha_3 \Gamma(w_s, w_s)] \phi_n'' \\ & - 2\alpha_3 \Gamma(w_s, \phi_n) w_s'' \\ & - \alpha_{61} \frac{2V_D^2}{(1-w_s)^3} \phi_n - \alpha_{62} \frac{2V_D^2}{(1+w_s)^3} \phi_n \\ & - \alpha_{71} \frac{3}{(1-w_s)^4} \phi_n - \alpha_{72} \frac{3}{(1+w_s)^4} \phi_n = 0 \end{aligned} \tag{42}$$

where $\phi_n(x)$ is the n th mode shape, and ω_n is the n th nondimensional natural frequency.

5 Perturbation analysis

In order to determine approximate solution of the nonlinear distributed parameter system, the multiple-scale

method is directly applied to the partial differential equation of motion and associated boundary conditions. Therefore, the second-order uniform solution is expressed in the form of [52]:

$$\begin{aligned} u(x, t; \varepsilon) = & \varepsilon u_1(x, T_0, T_1, T_2) + \varepsilon^2 u_2(x, T_0, T_1, T_2) \\ & + \varepsilon^3 u_3(x, T_0, T_1, T_2) + \dots \end{aligned} \tag{43}$$

where ε is a small dimensionless book keeping parameter and $T_0 = t$, $T_1 = \varepsilon t$ and $T_2 = \varepsilon^2 t$ are different timescales. Using chain rule, time derivatives can be written as:

$$\begin{aligned} \frac{d}{dt} & = D_0 + \varepsilon D_1 + \varepsilon^2 D_2 + \dots \\ \frac{d^2}{dt^2} & = D_0 + 2\varepsilon D_0 D_1 + \varepsilon^2 (D_1^2 + 2D_0 D_2) + \dots \end{aligned} \tag{44}$$

where $D_n = \partial/\partial T_n$. In order to investigate the principle parametric resonances of the system, the damping coefficient and the excitation amplitude are scaled as:

$$C = \varepsilon^2 C, \quad V_{AC} = \varepsilon^2 V_{AC} \tag{45}$$

Substituting Eqs. (43)–(45) into Eq. (40) and equating the terms of like powers of ε , the following results are achieved:

$$\begin{aligned} O(\varepsilon) : L(u_1) = & D_0^2 u_1 + u_1^{IV} + \alpha_4 \ddot{u}_1'' \\ & - [\alpha_1 + \alpha_2 + \alpha_3 \Gamma(w_s, w_s)] u_1'' - 2\alpha_3 \Gamma(w_s, u_1) w_s'' \\ & - \frac{2\alpha_{61} V_D^2}{(1-w_s)^3} u_1 - \frac{2\alpha_{62} V_D^2}{(1+w_s)^3} u_1 - \frac{3\alpha_{71}}{(1-w_s)^4} u_1 \\ & - \frac{3\alpha_{72}}{(1+w_s)^4} u_1 = 0 \end{aligned} \tag{46}$$

$$\begin{aligned} O(\varepsilon^2) : L(u_2) = & -2D_0 D_1 u_1 - 2\alpha_4 D_0 D_1 u_1'' \\ & + 2\alpha_3 \Gamma(w_s, u_1) u_1'' + \alpha_3 \Gamma(u_1, u_1) w_s'' \\ & + \frac{3\alpha_{61} V_D^2}{(1-w_s)^4} u_1^2 - \frac{3\alpha_{62} V_D^2}{(1+w_s)^4} u_1^2 + \frac{6\alpha_{71}}{(1-w_s)^5} u_1^2 \\ & - \frac{6\alpha_{72}}{(1+w_s)^5} u_1^2 + 2P_1(x) \cos(\Omega T_0) \end{aligned} \tag{47}$$

$$\begin{aligned} O(\varepsilon^3) : L(u_3) = & -2D_0 D_1 u_2 - D_1^2 u_1 - 2D_0 D_2 u_1 \\ & - C D_0 u_1 - \alpha_4 (2D_0 D_1 u_2'' + 2D_0 D_2 u_1'' + D_1^2 u_1'') \\ & + 2\alpha_3 \Gamma(u_1, u_2) w_s'' + \alpha_3 \Gamma(u_1, u_1) u_1'' \\ & + 2\alpha_3 \Gamma(w_s, u_1) u_2'' + 2\alpha_3 \Gamma(w_s, u_2) u_1'' \\ & + \frac{6\alpha_{61} V_D^2}{(1-w_s)^4} u_1 u_2 - \frac{6\alpha_{62} V_D^2}{(1+w_s)^4} u_1 u_2 \\ & + \frac{12\alpha_{71}}{(1-w_s)^5} u_1 u_2 - \frac{12\alpha_{72}}{(1+w_s)^5} u_1 u_2 + \frac{4\alpha_{61} V_D^2}{(1-w_s)^5} u_1^3 \end{aligned}$$

$$\begin{aligned}
 & + \frac{4\alpha_{62} V_D^2}{(1+w_s)^5} u_1^3 + \frac{10\alpha_{71}}{(1-w_s)^6} u_1^3 \\
 & + \frac{10\alpha_{72}}{(1+w_s)^6} u_1^3 + 4P_2(x) \cos(\Omega T_0)
 \end{aligned} \tag{48}$$

where

$$P_1(x) = \frac{\alpha_{61} V_D V_{AC}}{(1-w_s)^2}, \quad P_2(x) = \frac{\alpha_{61} V_D V_{AC}}{(1-w_s)^3} \tag{49}$$

The boundary conditions are similar for all orders and are given by:

$$u(x = 0, 1) = 0 \text{ and } u'(x = 0, 1) = 0 \tag{50}$$

The general solution of Eq. (46) and the associated boundary conditions can be expressed as:

$$u_1 = A(T_1, T_2)e^{i\omega T_0} \phi(x) + \bar{A}(T_1, T_2)e^{-i\omega T_0} \phi(x) \tag{51}$$

where $\phi(x)$ and ω are the mode shape and the corresponding natural frequency for the considered mode, respectively. Substituting Eq. (51) into Eq. (47) and considering the solvability condition, one realizes that A is just the slow timescale complex-valued function, i.e., $A = A(T_2)$, which can be obtained by applying the solvability conditions at third order. By eliminating the secular terms, the second-order equation reduces to:

$$\begin{aligned}
 L(u_2) = & \left(A^2 e^{2i\omega T_0} + 2A\bar{A} + \bar{A}^2 e^{-2i\omega T_0} \right) h(x) \\
 & + 2P_1(x) \cos(\Omega T_0)
 \end{aligned} \tag{52}$$

where $h(x)$ is defined as follows:

$$\begin{aligned}
 h(x) = & 2\alpha_3 \Gamma(w_s, \phi) \phi'' + \alpha_3 \Gamma(\phi, \phi) w_s'' \\
 & + \frac{3\alpha_{61} V_D^2}{(1-w_s)^4} \phi^2 - \frac{3\alpha_{62} V_D^2}{(1+w_s)^4} \phi^2 \\
 & + \frac{6\alpha_{71}}{(1-w_s)^5} \phi^2 - \frac{6\alpha_{72}}{(1+w_s)^5} \phi^2
 \end{aligned} \tag{53}$$

The solution of the second-order equation can be found in the form of:

$$\begin{aligned}
 u_2 = & \psi_1(x) A^2 e^{2i\omega T_0} + 2\psi_2(x) A\bar{A} + \psi_1(x) \bar{A}^2 e^{-2i\omega T_0} \\
 & + \psi_3(x) \left(e^{i\Omega T_0} + e^{-i\Omega T_0} \right)
 \end{aligned} \tag{54}$$

where $\psi_1(x)$, $\psi_2(x)$, and $\psi_3(x)$ are the solutions of the following boundary value problems:

$$\begin{aligned}
 \psi_1^{IV} - 4\omega^2 \psi_1 - 4\alpha_4 \omega^2 \psi_1'' - [\alpha_1 + \alpha_2 \\
 + \alpha_3 \Gamma(w_s, w_s)] \psi_1'' - 2\alpha_3 \Gamma(w_s, \psi_1) w_s'' \\
 - \frac{2\alpha_{61} V_D^2}{(1-w_s)^3} \psi_1 - \frac{2\alpha_{62} V_D^2}{(1+w_s)^3} \psi_1 \\
 - \frac{3\alpha_{71}}{(1-w_s)^4} \psi_1 - \frac{3\alpha_{72}}{(1+w_s)^4} \psi_1 = 2\alpha_3 \Gamma(w_s, \phi) \phi'' \\
 + \alpha_3 \Gamma(\phi, \phi) w_s'' + \frac{3\alpha_{61} V_D^2}{(1-w_s)^4} \phi^2 - \frac{3\alpha_{62} V_D^2}{(1+w_s)^4} \phi^2 \\
 + \frac{6\alpha_{71}}{(1-w_s)^5} \phi^2 - \frac{6\alpha_{72}}{(1+w_s)^5} \phi^2
 \end{aligned} \tag{55}$$

$$\begin{aligned}
 \psi_2^{IV} - [\alpha_1 + \alpha_2 + \alpha_3 \Gamma(w_s, w_s)] \psi_2'' \\
 - 2\alpha_3 \Gamma(w_s, \psi_2) w_s'' \\
 - \frac{2\alpha_{61} V_D^2}{(1-w_s)^3} \psi_2 - \frac{2\alpha_{62} V_D^2}{(1+w_s)^3} \psi_2 - \frac{3\alpha_{71}}{(1-w_s)^4} \psi_2 \\
 - \frac{3\alpha_{72}}{(1+w_s)^4} \psi_2 = 2\alpha_3 \Gamma(w_s, \phi) \phi'' \\
 + \alpha_3 \Gamma(\phi, \phi) w_s'' + \frac{3\alpha_{61} V_D^2}{(1-w_s)^4} \phi^2 - \frac{3\alpha_{62} V_D^2}{(1+w_s)^4} \phi^2 \\
 + \frac{6\alpha_{71}}{(1-w_s)^5} \phi^2 - \frac{6\alpha_{72}}{(1+w_s)^5} \phi^2
 \end{aligned} \tag{56}$$

$$\begin{aligned}
 \psi_3^{IV} - \Omega^2 \psi_3 - \alpha_4 \Omega^2 \psi_3'' \\
 - [\alpha_1 + \alpha_2 + \alpha_3 \Gamma(w_s, w_s)] \psi_3'' \\
 - 2\alpha_3 \Gamma(w_s, \psi_3) w_s'' \\
 - \frac{2\alpha_{61} V_D^2}{(1-w_s)^3} \psi_3 - \frac{2\alpha_{62} V_D^2}{(1+w_s)^3} \psi_3 - \frac{3\alpha_{71}}{(1-w_s)^4} \psi_3 \\
 - \frac{3\alpha_{72}}{(1+w_s)^4} \psi_3 = P_1(x)
 \end{aligned} \tag{57}$$

In the case of principle parametric resonance, in order to show the nearness of the excitation frequency Ω to twice of the natural frequency ω , detuning parameter σ is described in the form of:

$$\Omega = 2\omega + \varepsilon^2 \sigma \tag{58}$$

Substituting Eqs. (51), (54), and (58) into Eq. (48) yields to:

$$\begin{aligned}
 L(u_3) = & \left[-i\omega (2A'(\phi + \alpha_4 \phi'') + AC\phi) + \chi(x) A^2 \bar{A} \right. \\
 & \left. + \xi(x) \bar{A} e^{i\sigma T_2} \right] e^{i\omega T_0} + c.c. + NST
 \end{aligned} \tag{59}$$

where A' is the derivative of A with respect to T_2 , and $c.c.$ denotes the complex conjugate of prior terms, and

NST denotes nonsecular terms. The functions $\chi(x)$ and $\xi(x)$ are defined in the ‘‘Appendix.’’ Since the corresponding homogeneous problem of Eq. (59) is self-adjoint (the adjoints are $\phi(x)e^{\pm i\omega T_0}$), the solvability conditions can be obtained by multiplying the right-hand side of Eq. (59) by $\phi(x)e^{-i\omega T_0}$ and integrating the outcome from $x = 0$ to $x = 1$, as follows:

$$i\omega(2mA' + \mu A) + 8SA^2\bar{A} - F\bar{A}e^{i\sigma T_2} = 0 \tag{60}$$

where

$$\begin{aligned} \mu &= \int_0^1 C\phi^2(x)dx, \\ m &= \int_0^1 (\phi^2(x) + \alpha_4\phi''(x)\phi(x))dx, \\ S &= -\frac{1}{8}\int_0^1 \chi(x)\phi(x)dx, \quad F = \int_0^1 \xi(x)\phi(x)dx. \end{aligned} \tag{61}$$

Expressing A in the polar form is as follows:

$$A = \frac{1}{2}a(T_2)e^{i\beta(T_2)} \tag{62}$$

where a and β are real-valued functions of T_2 representing the amplitude and the phase of the response, respectively. Substituting Eq. (62) into Eq. (60) and separating the real and imaginary parts, and introducing $\gamma = \sigma T_2 - 2\beta$, the modulation equations can be expressed as:

$$\begin{aligned} a' &= -\frac{1}{2}\frac{\mu a}{m} + \frac{1}{2}\frac{Fa \sin(\gamma)}{\omega m} \\ a\gamma' &= -\frac{2Sa^3}{\omega m} + \frac{Fa \cos(\gamma)}{\omega m} + \sigma a \end{aligned} \tag{63}$$

The steady-state response can be determined using the fact that a' and γ' are constants in the steady state. Hence, letting $a' = \gamma' = 0$ in Eq. (63), one obtains the fix points (a_0, γ_0) of the system. Consequently, the frequency response function can be obtained by eliminating γ_0 from the achieved equations, as follows:

$$(2Sa_0^3 - \sigma\omega ma_0)^2 + \omega^2\mu^2 a_0^2 = F^2 a_0^2 \tag{64}$$

According to Eq. (64), there are two possibilities of solutions: trivial response ($a_0 = 0$) and nontrivial response ($a_0 \neq 0$). The stability of the nontrivial periodic solutions of Eq. (64) can be determined by evaluating the eigenvalues of the Jacobian matrix of Eq. (63) at fixed points (a_0, γ_0) , given by:

$$\begin{bmatrix} \frac{1}{2}\frac{F \sin(\lambda_0) - \omega\mu}{\omega m} & \frac{1}{2}\frac{Fa_0 \cos(\lambda_0)}{\omega m} \\ -\frac{4Sa_0}{\omega m} & -\frac{F \sin(\lambda_0)}{\omega m} \end{bmatrix} \tag{65}$$

It is convenient to determine the stability of the trivial fixed points from the Cartesian form of the modulation equation rather than the Polar form. Introducing $A = \frac{1}{2}(p - iq)e^{i\nu(T_2)}$ into Eq. (60), and separating the real and imaginary parts, modulation equation in the Cartesian form can be obtained as:

$$\begin{aligned} p' &= \frac{S}{\omega m}(p^2q + q^3) - \frac{1}{2}\frac{\mu p}{m} - \left(\frac{1}{2}\frac{F}{\omega m} - \nu\right)q \\ q' &= -\frac{S}{\omega m}(p^3 + pq^2) - \frac{1}{2}\frac{\mu q}{m} - \left(\frac{1}{2}\frac{F}{\omega m} + \nu\right)p \end{aligned} \tag{66}$$

where p and q are real-valued functions and $\nu = \frac{1}{2}\sigma$. The stability of the trivial fixed points can be determined by evaluating the eigenvalues of the Jacobian matrix of Eq. (66) at trivial state $p_0 = q_0 = 0$.

6 Results and discussion

In this section, the numerical results are presented. The numerical simulations are performed for the case study of the PZT-5H nanobeam, with physical properties listed in Table 1 (mechanical properties of the surface layer were adopted from [53]).

Figure 2 shows the effect of the surface energy on the variation in the normalized distance between the nanobeam midpoint and the substrate versus the applied DC voltage. The piezoelectric polarization voltage is considered to be zero. As it can be seen, surface effects can remarkably influence the pull-in voltages. It is seen that in the presence of the surface effects pull-in occurs at $V_{DC} \approx 3.42$ V, while in the absence of the surface effects, pull-in occurs at $V_{DC} \approx 2.32$ V.

Table 1 Physical properties of the nanobeam

$L = 1$ nm	$E^s = 7.56$ N/m
$b = 6$ nm	$\rho^s = 7.5 \times 10^{-6}$ kg/m ²
$h = 4$ nm $l_u = 80$ nm	$\tau_0 = 1$ N/m
$l_d = 20$ nm	$\nu = 0.31$
$g_0 = 4$ nm	$\bar{e}_{31} = -6.55$ C/m ²
$E = 126$ GPa	$\epsilon_0 = 8.854 \times 10^{-12}$ F/m
$\rho = 7500$ kg/m ³	

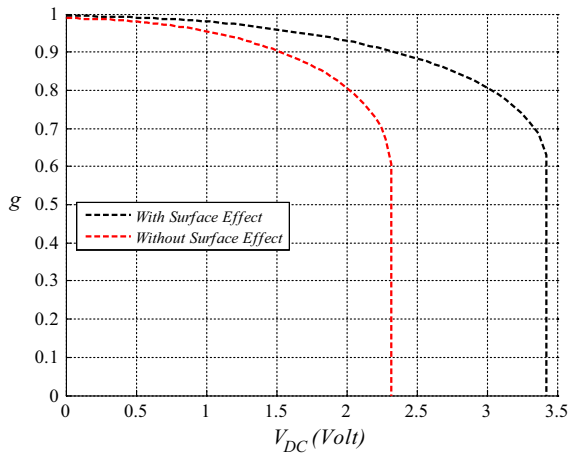


Fig. 2 Influence of the surface effects on the normalized midpoint static deflection for various values of V_{DC} ; $V_P = 0$ V

This result is based on the fact that the surface effect increases the stiffness of the nanobeam. In addition, the surface effect has also a significant influence on the midpoint static deflection of the nanobeam. It can be found that the central displacement of the nanobeam in the presence of the surface effects is always less than the central displacement in the absence of the surface effects for any applied DC voltage prior to the pull-in instability.

Figure 3 illustrates the gap between the midpoint and the substrate while varying the DC voltage for the three different piezoelectric actuation voltages. This figure shows that piezoelectric actuation with positive polarity increases the pull-in voltage, since it generates tensile axial force and increases the nanobeam stiffness. Negative polarity has just a diverse effect, since it generates compression axial load in the nanobeam. As it can be seen, the piezoelectric actuation significantly shifts the equilibrium manifolds and consequently the pull-in voltages. For example, pull-in occurs at $V_{DC} \approx 3.81$ V for the positive polarity $V_P = 0.2$ V compared to $V_{DC} = 3.02$ V for the negative polarity equal to $V_P = -0.2$ V. It is noted that piezoelectric actuation can be considered as a design parameter to control the system pull-in instability.

Figure 4 depicts the effect of van der Waals forces on the normalized maximum midpoint static deflection of the nanobeam. This figure shows the obtained results in the absence and presence of the van der Waals forces for $V_P = 0$ V, and two different initial gaps $g_0 = 4$ nm and $g_0 = 2$ nm. As it can be seen, while $g_0 = 4$ nm two

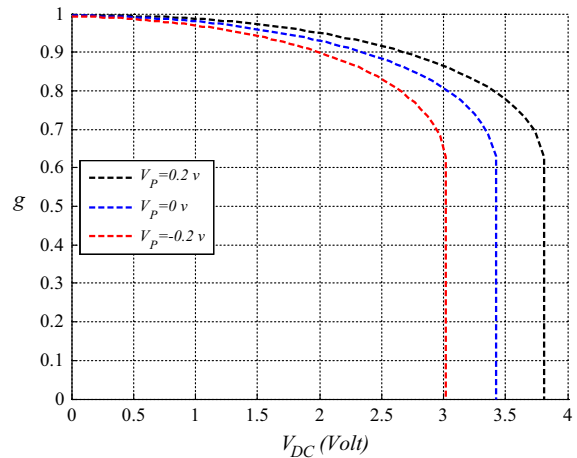


Fig. 3 Normalized midpoint static deflection versus V_{DC} , for three different values of piezoelectric voltages

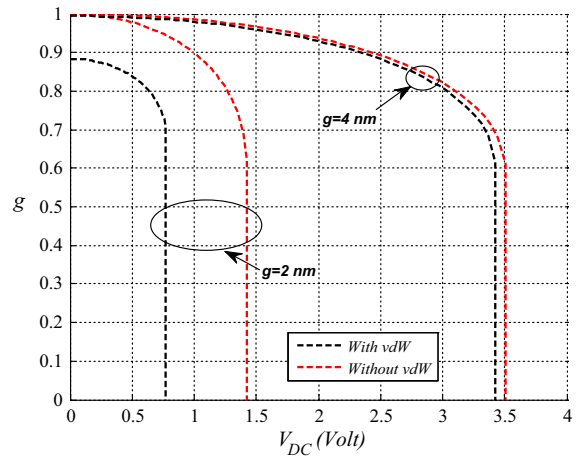


Fig. 4 Influence of the van der Waals forces on the midpoint normalized static deflection for various values of V_{DC} ; $V_P = 0$ V

curves differ slightly from each other, hence, the van der Waals forces do not provide considerable effects on the equilibrium positions in this case. However, while the gap width is equal to 2 nm, van der Waals forces significantly affect the pull-in voltages and the equilibrium positions. As it is seen, by considering the van der Waals forces, pull-in occurs at $V_{DC} \approx 0.77$ V; however, by neglecting the van der Waals forces, pull-in occurs at $V_{DC} \approx 1.42$ V. This remarkable influence can be due to the fact that the van der Waals forces dominate the midplane stretching for the smaller initial gaps. It is worth mentioning that there exists rather too much static deflection while no DC voltage is applied. This

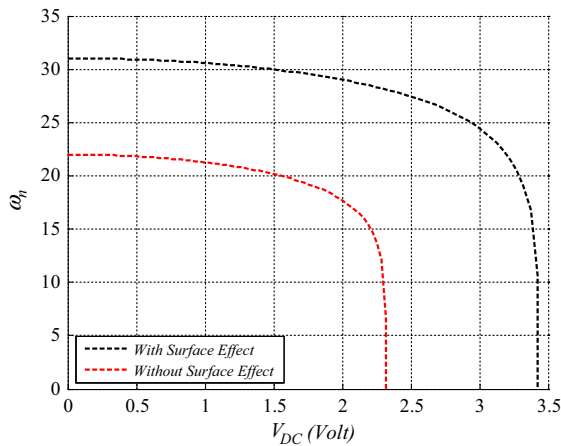


Fig. 5 Influence of the surface effects on the fundamental natural frequency of the nanobeam for various values of V_{DC} ; $V_P = 0$ V

deflection is due to the electrostatic interactions among the magnetic dipoles at the atomic scales. It is worthy to note that in the following results, the 4 nm initial gap is used.

Figure 5 shows the influence of the surface effects on the fundamental natural frequency of the piezoelectric nanobeam for various values of the DC voltage. The piezoelectric polarization voltage is considered to be zero. As it can be seen, fundamental natural frequency of the nanobeam decreases monotonically until it suddenly reaches the zero where it escapes to the substrate (i.e., pull-in instability). This Fig. 5 also indicates that the surface effects have significantly influenced the natural frequency and the pull-in voltage as they are increased in the presence of the surface effects.

Figure 6 shows the influence of the piezoelectric actuation on the fundamental natural frequency. Piezoelectric actuation significantly affects the natural frequency of the nanobeam. As the piezoelectric polarity increases, the pull-in voltage and the fundamental natural frequency increase. Fundamental natural frequency decreases monotonically until it reaches the pull-in point for all cases.

Figure 7 illustrates the frequency–response curve of the piezoelectric nanobeam near the principal parametric resonance in the presence of the surface effects. The response of nanoresonator is investigated for $V_{DC} = 1$ V, $V_P = 0$ V, $V_{AC} = 0.9$ V, and the quality factor of $Q = 1000$. The damping coefficient is related to the quality factor by $Q = \omega_1/C$, where ω_1 is the fundamental natural frequency of the nanobeam. The

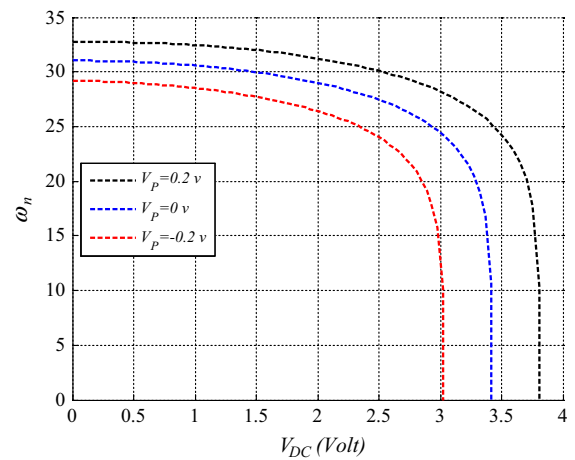


Fig. 6 Influence of the different piezoelectric actuation levels on the fundamental natural frequency of the nanobeam for various values of V_{DC}

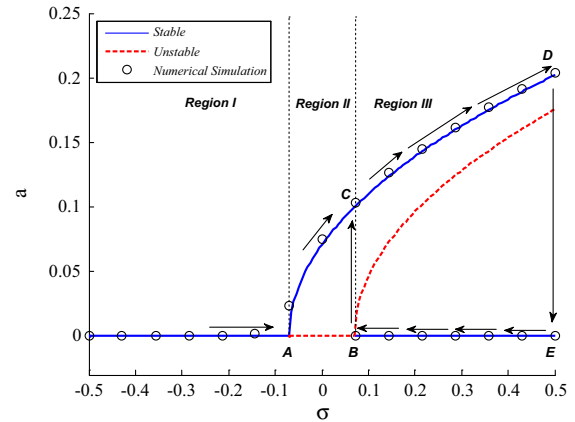


Fig. 7 Frequency–response curve near principal parametric resonance; $V_{DC} = 1$ V, $V_P = 0.0$ V, and $V_{AC} = 0.9$ V

parametric frequency–amplitude curve consists of one trivial branch and two nontrivial steady-state branches. It is seen that frequency–response branches are tilted to the right, which represents a hardening-like behavior.

Figure 7 depicts a sharp transition between the trivial response and the large-amplitude subharmonic response due to the parametric excitation. For certain values of the excitation frequency, there are multiple stationary solutions. According to Fig. 7, in the region I, the system has only one trivial stable solution. In the second region, there exist two possibilities for the solution, one unstable trivial solution and a stable non-trivial solution. For excitations in the region III, the system has a single stable trivial solution and two non-

trivial solutions, one stable and one unstable. The system may lay on either branches depending on the initial conditions. The existence of the stable and unstable manifolds in the multi-valued frequency–response curves results in bifurcations in the system. As it is seen, while the frequency is swept up, the response of the system remains trivial until it reaches the supercritical pitchfork bifurcation point *A* where the parametric response is activated. At this point, a new stable nontrivial branch appears in the response while the trivial solution loses the stability. As sweeping continues, at subcritical pitchfork bifurcation point *B*, the trivial solution turns stable and another unstable nontrivial solution appears. Depending on the initial conditions, response may lay on either the upper or the lower branches. In addition, forward and backward frequency sweeps result in jumps and hysteresis in the response. For instance, a forward sweep passing point *D* results in a jump to the lower stable branch and a backward sweep passing point *B* results in a jump to the upper stable branch. This region also indicates the hysteretic response in the nanobeam. As it is seen, the numerical results are in good agreement with the perturbation results.

Figure 8 shows the trivial state stability boundaries as a function of AC voltage for two different values of damping parameter and $V_{DC} = 1\text{ V}$, $V_P = 0\text{ V}$ while considering the surface effects. The region inside the wedge denotes the instability zone, which along its boundaries, the catastrophic bifurcations occur. Points *A* and *B* are the pitchfork bifurcations corresponding to Fig. 7. As it is seen, increasing the AC voltage results in increasing the instability zone width. Note that the damping raises the instability region, and it rounds off the V-shape region bottom, so a nonzero voltage is needed for transition to instability.

Figure 9 illustrates the effect of surface energy on the principal parametric resonance. It follows from the figure that the influence of the surface effect is remarkable. As it is seen, surface effect significantly reduces the stable nontrivial manifold amplitude, whereas it has slightly altered the unstable nontrivial manifold. Generally speaking, considering the surface effects leads to a reduction in the parametric response. It is seen that the trivial unstable response is triggered between $-0.125 < \sigma < 0.125$ in the absence of the surface effects compared to $-0.07 < \sigma < 0.07$ in the presence of the surface effects. It is due to the fact that surface effect increases the bending stiffness and amplifies the

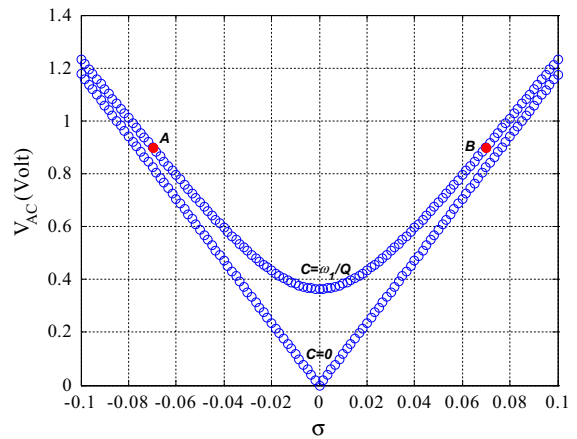


Fig. 8 Trivial state stability boundaries as a function of AC voltage for two different values of damping parameter; $V_{DC} = 1\text{ V}$, $V_P = 0\text{ V}$

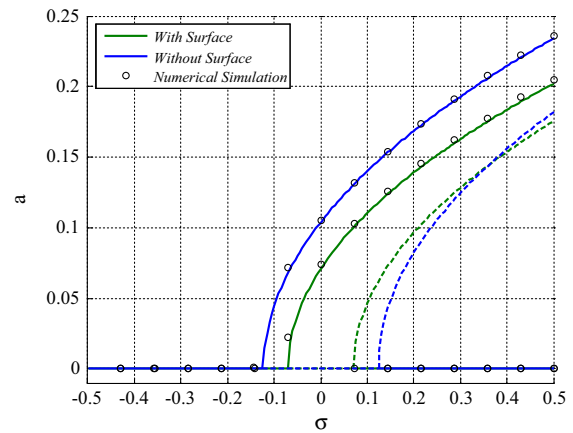


Fig. 9 Influence of the surface effects on the parametric frequency–response curves; $V_{DC} = 1\text{ V}$, $V_P = 0\text{ V}$ and $V_{AC} = 0.9\text{ V}$

geometric nonlinearity which reduces the parametric response region. As Fig. 9 exhibits, the surface effect significantly alters the locus of the bifurcation points (significantly shifted toward the $\sigma = 0$) and the hysteresis region which can lead to serious consequences on the stability of the nanoresonator. To validate the perturbation results, numerical simulation is carried out, and as it can be seen, analytical results are in excellent agreement with those obtained by numerical simulation.

Influence of different piezoelectric voltages on the parametric resonance is investigated in Fig. 10. The surface effect is considered for all cases. It is seen that the frequency–response curves are of hardening type.

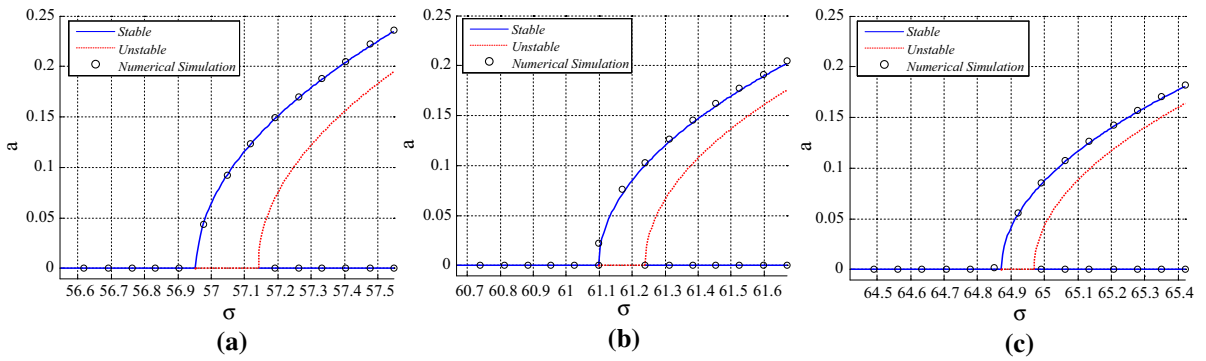


Fig. 10 Frequency–response curves for different levels of the piezoelectric voltages representing hardening effect; $V_{DC} = 1\text{ V}$, $V_{AC} = 0.9\text{ V}$, **a** $V_p = -0.2\text{ V}$, **b** $V_p = 0.0\text{ V}$, **c** $V_p = 0.2\text{ V}$

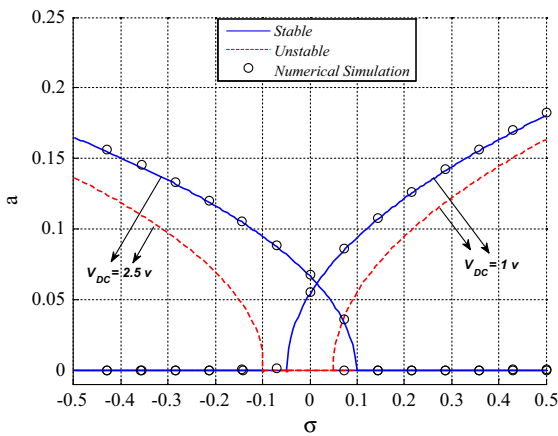


Fig. 11 Influence of the different DC voltages on the parametric frequency–response curves; $V_p = 0\text{ V}$ and $V_{AC} = 0.9\text{ V}$

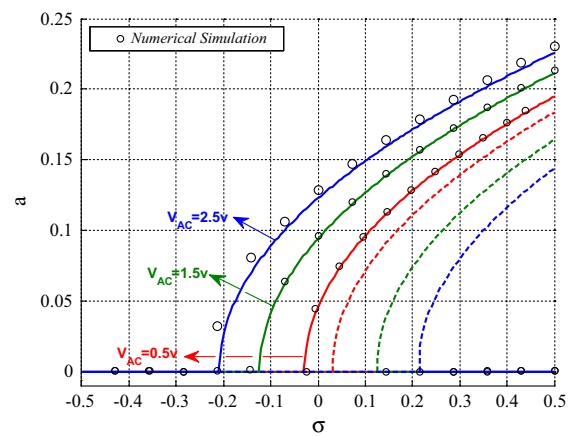


Fig. 12 Influence of the different AC voltages on the parametric frequency–response curves; $V_p = 0\text{ V}$ and $V_{DC} = 1\text{ V}$

According to Fig. 10, the parametric response region and the bifurcation points’ loci are strongly affected by the polarity of the piezoelectric actuation. As it is seen, the negative polarity actuation enhances the parametric response of the nanobeam and shifts the frequency–response curve to the left (see Fig. 10(a)). It also increases the zero-solution instability zone. As the piezoelectric polarity increases, the nontrivial manifold amplitude decreases. As mentioned before, it is due to the fact that positive piezoelectric polarization increases the system stiffness. The positive polarity actuation just has the opposite effect and shifts the frequency–response curve to the right of the frequency axis (see Fig. 10(c)). In all cases, two jumps occur in the system. It is worth mentioning that piezoelectric actuation can be used as a possible method for improving the signal-to-noise ratio and modulating the response.

Figure 11 represents the frequency–response curves near the principal parametric resonance for two different levels of the DC voltage actuation and $V_p = 0\text{ V}$, $V_{AC} = 0.9\text{ V}$. It can be found that increasing the DC voltage load leads to the softening behavior of the nanoresonator. Since, the softening effect of the electrostatic nonlinearity dominates the hardening effect of the geometric nonlinearity. This figure exhibits that increasing the DC voltage decreases the stable and the unstable nonzero solution manifold amplitudes. It is seen that increasing the DC voltage level significantly increases the trivial solution instability region and affects the pitchfork bifurcation points’ loci. The analytical results are in excellent agreement with those obtained by numerical simulation.

Figure 12 shows the influence of the AC voltage actuation on the parametric frequency–response curves

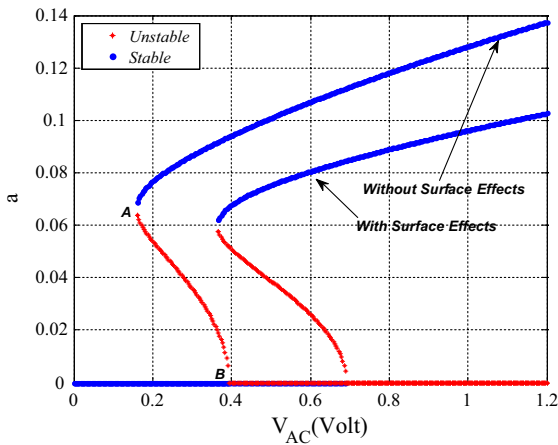


Fig. 13 Influence of the surface effects on the force–response curves; $V_{DC} = 1$ V, $V_P = 0$ V and $\sigma = 0.05$

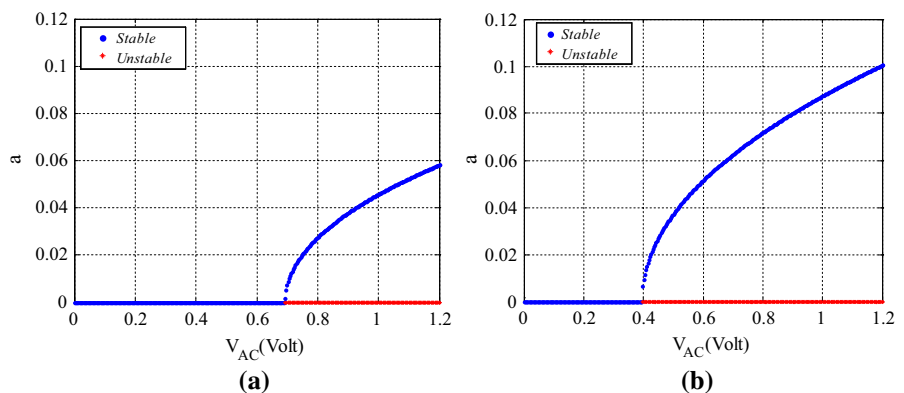
for $V_{DC} = 1$ V and $V_P = 0$ V. As it is seen, increasing the AC voltage actuation increases the stable nonzero solution manifold amplitude and decreases the unstable nonzero solution manifold amplitude. It also increases the frequency band which the nanoresonator settles to unstable zero-amplitude solution. It illustrates that, by increasing the AC voltage load, the supercritical pitchfork bifurcation points significantly shift to lower frequencies, whereas subcritical bifurcation points shift to higher frequencies. According to this figure, numerical simulation and the perturbation results are in excellent agreement for $V_{AC} = 0.5$ V and $V_{AC} = 1.5$ v while there is a slight difference between the analytical and the numerical methods in predicting the response amplitude for $V_{AC} = 2.5$ V. As it is seen, perturbation method fails to predict the system behavior for higher levels of the AC voltage actuation. Hence, an alternative technique such as the shooting method is

recommended to capture the precise global behavior of the nanoresonator.

Figure 13 shows the influence of the surface effects on the characteristic curves of the response amplitude versus the excitation amplitude V_{AC} corresponding to static loading of Fig. 7 and $\sigma = 0.05$. As it is seen, both curves are qualitatively similar. For instance, in the absence of the surface effects and $0.16 < V_{AC} < 0.39$, there are three solutions, one stable trivial solution and two nontrivial solutions one of which is stable. There appear two bifurcation points in the response, i.e., the saddle-node bifurcation point A and the subcritical pitchfork bifurcation point B. As V_{AC} is increased, the amplitude remains zero until it reaches the bifurcation point B, as V_{AC} is increased further, a sudden jump takes place from point B to the upper stable branch. By reversing this procedure, the solution decreases slowly along the upper branch as it reaches the saddle-node bifurcation point A, where it experiences a jump down to the lower stable branch. It can be found that in the presence of the surface effects, the parametric response profoundly decreases and also the bifurcation points’ loci shift to the right.

Figure 14 shows force–response curves in the presence and absence of the surface effects for the parameters of Fig. 7 and $\sigma = -0.05$, respectively. As it is seen, both diagrams are qualitatively similar. Different detuning parameters lead to different solutions. For instance, according to the Fig. 14a, when $\sigma < 0.69$, there is just a stable zero solution. Above this threshold (supercritical pitchfork bifurcation point), there are two solutions: a stable nonzero solution and an unstable zero solution. As V_{AC} is increased slowly, the amplitude remains zero until it reaches the bifurcation point. As V_{AC} is increased further, the response amplitude grows

Fig. 14 Influence of the surface effects on the force–response curves; $V_{DC} = 1$ V, $V_P = 0$ V and $\sigma = -0.05$, **a** considering the surface effects, **b** neglecting the surface effects



along the upper stable branch. By reversing this procedure, the solution decreases slowly along the upper stable nontrivial branch as it reaches the bifurcation point and the zero amplitude. The system would experience neither a jump nor a hysteresis in this case. It can be found that in the presence of the surface effects, the parametric response profoundly decreases and also the bifurcation point loci shift to the right.

7 Conclusions

In this paper, the parametric oscillations of an electrostatically actuated clamped–clamped piezoelectric nanoresonator considering surface effects were studied. The governing equation of motion was derived using the extended Hamilton principle. The static equilibria of the nanobeam under DC voltage loads were investigated using Galerkin method. Fundamental natural frequencies of the nanobeam were calculated using the ROM for different values of the DC voltages. It was shown that the effect of the van der Waals force on the static equilibria and the pull-in voltage was remarkable for nanoresonators of very small gaps. The results show that by neglecting the dissipative forces, the pull-in voltage is overestimated. The results also suggest that piezoelectric actuation can be used as a design parameter to control the static response and pull-in instability by changing the nanobeam bending stiffness. This study revealed that surface effect profoundly shifts the fundamental natural frequencies, static equilibria, and pull-in voltages, and hence, it is necessary to consider them for modeling and design of the nanoresonators. Dynamic response of the nanobeam near principle parametric resonance was studied using the multiple-scale method. The results indicated a reduction in parametric response amplitude and unstable trivial region in the presence of the surface effects. This study revealed that surface effects significantly shifts the pitchfork bifurcation points' loci and affects nonlinear phenomena such as jump and hysteresis. Accordingly, it is needed to consider surface effects for more accurate simulation and modeling of the nanoresonator. Frequency–response curves have been plotted for different voltage loads. It was shown that increasing the DC load decreases parametric response amplitude and increases the unstable zero-solution region. Moreover, it could lead to softening type behavior, as the nonlinear electrostatic term dominates the geomet-

ric nonlinearity effect. It was showed that increasing the AC voltage load enhances the parametric response amplitude. The results revealed that piezoelectric actuation could be used as a possible method for improving the signal-to-noise ratio and modulating the response. Numerical simulations have been performed to validate the perturbation results. It has been found that the results are in a good agreement with each other for small enough AC voltage amplitudes. The presented results and modeling approach can be used in the design and optimization of novel NEMS resonators.

Appendix

$$\begin{aligned}
 S &= 3\alpha_3 \Gamma(\phi, \phi) \phi'' + 2\alpha_3 \Gamma(\phi, w_s) \psi_1'' \\
 &+ 2\alpha_3 \Gamma(w_s, \psi_1) \phi'' + 2\alpha_3 \Gamma(\phi, \psi_1) w_s'' \\
 &+ 4\alpha_3 \Gamma(\phi, w_s) \psi_2'' + 4\alpha_3 \Gamma(w_s, \psi_2) \phi'' \\
 &+ 4\alpha_3 \Gamma(\phi, \psi_2) w_s'' \\
 &+ 6 \frac{\alpha_{61} V_D^2 \phi \psi_1}{(1-w_s)^4} - 6 \frac{\alpha_{62} V_D^2 \phi \psi_1}{(1+w_s)^4} + 12 \frac{\alpha_{61} V_D^2 \phi \psi_2}{(1-w_s)^4} \\
 &- 12 \frac{\alpha_{62} V_D^2 \phi \psi_2}{(1+w_s)^4} + 12 \frac{\alpha_{61} V_D^2 \phi^3}{(1-w_s)^5} + 12 \frac{\alpha_{62} V_D^2 \phi^3}{(1+w_s)^5} \\
 &+ 12 \frac{\alpha_{71} V_D^2 \phi \psi_1}{(1-w_s)^5} - 12 \frac{\alpha_{72} V_D^2 \phi \psi_1}{(1+w_s)^5} + 24 \frac{\alpha_{71} V_D^2 \phi \psi_2}{(1-w_s)^5} \\
 &- 24 \frac{\alpha_{72} V_D^2 \phi \psi_2}{(1+w_s)^5} + 30 \frac{\alpha_{71} V_D^2 \phi^3}{(1-w_s)^6} + 30 \frac{\alpha_{72} V_D^2 \phi^3}{(1+w_s)^6} \\
 F &= 2\alpha_3 \Gamma(w_s, \psi_3) \phi'' + 2\alpha_3 \Gamma(\phi, \psi_3) w_s'' \\
 &+ 2\alpha_3 \Gamma(\phi, w_s) \psi_3'' + 6 \frac{\alpha_{61} V_D^2 \phi \psi_3}{(1-w_s)^4} \\
 &- 6 \frac{\alpha_{62} V_D^2 \phi \psi_3}{(1+w_s)^4} + 12 \frac{\alpha_{71} V_D^2 \phi \psi_3}{(1-w_s)^5} - 12 \frac{\alpha_{72} V_D^2 \phi \psi_3}{(1+w_s)^5}
 \end{aligned}$$

References

1. Caruntu, D.I., Martinez, I.: Reduced order model of parametric resonance of electrostatically actuated MEMS cantilever resonators. *Int. J. Non-linear Mech.* **66**, 28–32 (2014)
2. Rhoads, J.F., Kumar, V., Shaw, S.W., Turner, K.L.: The nonlinear dynamics of electromagnetically actuated microbeam resonators with purely parametric excitations. *Int. J. Non-linear Mech.* **55**, 79–89 (2013)
3. Abdel-Rahman, E.M., Nayfeh, A.H.: Secondary resonances of electrically actuated resonant microsensors. *J.*

- Micromech. Microeng. **13**, 491–501 (2003). doi:[10.1088/0960-1317/13/3/320](https://doi.org/10.1088/0960-1317/13/3/320)
4. Kacem, N., Baguet, S., Hentz, S., Dufour, R.: Pull-in retarding in nonlinear nanoelectromechanical resonators under superharmonic excitation. *J. Comput. Nonlinear Dyn.* **7**(2), 021011 (2012)
 5. Ouakad, H.M., Younis, M.I.: Nonlinear dynamics of electrically actuated carbon nanotube resonators. *J. Comput. Nonlinear Dyn.* **5**(January 2010), 011009 (2010). doi:[10.1115/1.4000319](https://doi.org/10.1115/1.4000319)
 6. Nayfeh, A.H., Balachandran, B.: *Applied Nonlinear Dynamics: Analytical, Computational and Experimental Methods*. Wiley, New York (1995)
 7. Younis, M.I.: *MEMS Linear and Nonlinear Statics and Dynamics: MemS Linear and Nonlinear Statics and Dynamics*, vol. 20. Springer, Berlin (2010)
 8. Kacem, N., Hentz, S., Pinto, D., Reig, B., Nguyen, V.: Nonlinear dynamics of nanomechanical beam resonators: improving the performance of NEMS-based sensors. *Nanotechnology* **20**(27), 275501–275501 (2009). doi:[10.1088/0957-4484/20/27/275501](https://doi.org/10.1088/0957-4484/20/27/275501)
 9. Azizi, S., Ghazavi, M.R., Rezazadeh, G., Ahmadian, I., Cetinkaya, C.: Tuning the primary resonances of a micro resonator, using piezoelectric actuation. *Nonlinear Dyn.* **76**, 839–852 (2013). doi:[10.1007/s11071-013-1173-4](https://doi.org/10.1007/s11071-013-1173-4)
 10. Nayfeh, A.H., Younis, M.I., Abdel-Rahman, E.M.: Dynamic pull-in phenomenon in MEMS resonators. *Nonlinear Dyn.* **48**, 153–163 (2007). doi:[10.1007/s11071-006-9079-z](https://doi.org/10.1007/s11071-006-9079-z)
 11. Najar, F., Nayfeh, A., Abdel-Rahman, E., Choura, S., El-Borgi, S.: Nonlinear analysis of MEMS electrostatic microactuators: primary and secondary resonances of the first mode*. *J. Vib. Control* **16**(9), 1321–1349 (2010)
 12. Alsaleem, F.M., Younis, M.I., Ouakad, H.M.: On the nonlinear resonances and dynamic pull-in of electrostatically actuated resonators. *J. Micromech. Microeng.* **19**(4), 45013–45013 (2009)
 13. Pourkiaee, S.M., Khadem, S.E., Shahgholi, M.: Nonlinear vibration and stability analysis of an electrically actuated piezoelectric nanobeam considering surface effects and intermolecular interactions. *J. Vib. Control.* (2015). doi:[10.1177/1077546315603270](https://doi.org/10.1177/1077546315603270)
 14. Najar, F., Nayfeh, aH, Abdel-Rahman, E.M., Choura, S., El-Borgi, S.: Dynamics and global stability of beam-based electrostatic microactuators. *J. Vib. Control* **16**(5), 721–748 (2010). doi:[10.1177/1077546309106521](https://doi.org/10.1177/1077546309106521)
 15. Ouakad, H.M., Younis, M.I.: Natural frequencies and mode shapes of slacked carbon nanotube NEMS resonators. In: *ASME 2010 International Design Engineering Technical Conferences and Computers and Information in Engineering Conference*, pp. 645–652. American Society of Mechanical Engineers (2010)
 16. Ouakad, H.M., Younis, M.I.: Forced Vibrations of Slacked Carbon Nanotube Resonators. In: *ASME 2010 International Mechanical Engineering Congress and Exposition*, pp. 435–443. American Society of Mechanical Engineers (2010)
 17. Ouakad, H.M., Younis, M.I.: Natural frequencies and mode shapes of initially curved carbon nanotube resonators under electric excitation. *J. Sound Vib.* **330**(13), 3182–3195 (2011)
 18. Ouakad, H.M., Younis, M.I.: Dynamic response of slacked single-walled carbon nanotube resonators. *Nonlinear Dyn.* **67**(2), 1419–1436 (2012)
 19. Rasekh, M., Khadem, S.E.: Pull-in analysis of an electrostatically actuated nano-cantilever beam with nonlinearity in curvature and inertia. *Int. J. Mech. Sci.* **53**(2), 108–115 (2011). doi:[10.1016/j.ijmecsci.2010.11.007](https://doi.org/10.1016/j.ijmecsci.2010.11.007)
 20. Hajnayeb, A., Khadem, S.E.: Nonlinear vibrations of a carbon nanotube resonator under electrical and van der Waals forces. *J. Comput. Theor. Nanosci.* **8**(8), 1527–1534 (2011). doi:[10.1166/jctn.2011.1846](https://doi.org/10.1166/jctn.2011.1846)
 21. Hajnayeb, a, Khadem, S.E.: Nonlinear vibration and stability analysis of a double-walled carbon nanotube under electrostatic actuation. *J. Sound Vib.* **331**(10), 2443–2456 (2012). doi:[10.1016/j.jsv.2012.01.008](https://doi.org/10.1016/j.jsv.2012.01.008)
 22. Ouakad, H.M., Najar, F., Hattab, O.: Nonlinear analysis of electrically actuated carbon nanotube resonator using a novel discretization technique. *Math. Probl. Eng.* **2013** (2013). doi:[10.1155/2013/517695](https://doi.org/10.1155/2013/517695)
 23. Alibeigloo, A., Emtehani, A.: Static and free vibration analyses of carbon nanotube-reinforced composite plate using differential quadrature method. *Meccanica* **50**(1), 61–76 (2015)
 24. Xu, T., Younis, M.I.: Nonlinear dynamics of carbon nanotubes under large electrostatic force. *J. Comput. Nonlinear Dyn.* **11**(2), 021009 (2016)
 25. Asemi, S., Farajpour, A., Mohammadi, M.: Nonlinear vibration analysis of piezoelectric nanoelectromechanical resonators based on nonlocal elasticity theory. *Compos. Struct.* **116**, 703–712 (2014)
 26. Alibeigloo, A., Liew, K.: Elasticity solution of free vibration and bending behavior of functionally graded carbon nanotube-reinforced composite beam with thin piezoelectric layers using differential quadrature method. *Int. J. Appl. Mech.* **7**(01), 1550002 (2015)
 27. Ke, L.-L., Wang, Y.-S., Wang, Z.-D.: Nonlinear vibration of the piezoelectric nanobeams based on the nonlocal theory. *Compos. Struct.* **94**(6), 2038–2047 (2012)
 28. Arani, A.G., Kolahchi, R., Zarei, M.S.: Visco-surface-nonlocal piezoelectricity effects on nonlinear dynamic stability of graphene sheets integrated with ZnO sensors and actuators using refined zigzag theory. *Compos. Struct.* **132**, 506–526 (2015)
 29. He, J., Lilley, C.M.: Surface effect on the elastic behavior of static bending nanowires. *Nano Lett.* **8**, 1798–1802 (2008). doi:[10.1021/nl0733233](https://doi.org/10.1021/nl0733233)
 30. Miller, R.E., Shenoy, V.B.: Size-dependent elastic properties of nanosized structural elements. *Nanotechnology* **11**, 139–147 (2000). doi:[10.1088/0957-4484/11/3/301](https://doi.org/10.1088/0957-4484/11/3/301)
 31. Eom, K., Park, H.S., Yoon, D.S., Kwon, T.: Nanomechanical resonators and their applications in biological/chemical detection: nanomechanics principles. *Phys. Rep.* **503**(4–5), 115–163 (2011). doi:[10.1016/j.physrep.2011.03.002](https://doi.org/10.1016/j.physrep.2011.03.002)
 32. Wang, K., Wang, B.: Timoshenko beam model for the vibration analysis of a cracked nanobeam with surface energy. *J. Vib. Control.* (2013). doi:[10.1177/1077546313513054](https://doi.org/10.1177/1077546313513054)
 33. Eltahir, Ma., Mahmoud, F.F., Assie, A.E., Meletis, E.I.: Coupling effects of nonlocal and surface energy on vibration analysis of nanobeams. *Appl. Math. Comput.* **224**, 760–774 (2013). doi:[10.1016/j.amc.2013.09.002](https://doi.org/10.1016/j.amc.2013.09.002)
 34. Fu, Y., Zhang, J.: Size-dependent pull-in phenomena in electrically actuated nanobeams incorporating surface energies. *Appl. Math. Model.* **35**, 941–951 (2011). doi:[10.1016/j.apm.2010.07.051](https://doi.org/10.1016/j.apm.2010.07.051)

35. Ma, J.B., Jiang, L., Asokanathan, S.F.: Influence of surface effects on the pull-in instability of NEMS electrostatic switches. *Nanotechnology* **21**, 505708–505708 (2010). doi:[10.1088/0957-4484/21/50/505708](https://doi.org/10.1088/0957-4484/21/50/505708)
36. Wang, K.F., Wang, B.L.: Influence of surface energy on the non-linear pull-in instability of nano-switches. *Int. J. Non-Linear Mech.* **59**, 69–75 (2014). doi:[10.1016/j.ijnonlinmec.2013.11.004](https://doi.org/10.1016/j.ijnonlinmec.2013.11.004)
37. Wang, G.F., Feng, X.Q.: Surface effects on the buckling of nanowires under uniaxial compression. *Appl. Phys. Lett.* **94**, 141913–141913 (2009). doi:[10.1063/1.3117505](https://doi.org/10.1063/1.3117505)
38. Yan, Z., Jiang, L.Y.: Surface effects on the vibration and buckling of piezoelectric nanoplates. *Europhys. Lett.* **99**(July), 27007–27007 (2012). doi:[10.1209/0295-5075/99/27007](https://doi.org/10.1209/0295-5075/99/27007)
39. Zhang, J., Wang, C.: Vibrating piezoelectric nanofilms as sandwich nanoplates. *J. Appl. Phys.* **111**(January), 2–7 (2012). doi:[10.1063/1.4709754](https://doi.org/10.1063/1.4709754)
40. Cha, S.N., Seo, J.S., Kim, S.M., Kim, H.J., Park, Y.J., Kim, S.W., Kim, J.M.: Sound-driven piezoelectric nanowire-based nanogenerators. *Adv. Mater.* **22**(42), 4726–4730 (2010)
41. Kumar, B., Kim, S.-W.: Energy harvesting based on semi-conducting piezoelectric ZnO nanostructures. *Nano Energy* **1**(3), 342–355 (2012)
42. Ramezani, A., Alasty, A., Akbari, J.: Closed-form solutions of the pull-in instability in nano-cantilevers under electrostatic and intermolecular surface forces. *Int. J. Solids Struct.* **44**(14), 4925–4941 (2007)
43. Batra, R.C., Porfiri, M., Spinello, D.: Effects of van der Waals force and thermal stresses on pull-in instability of clamped rectangular microplates. *Sensors* **8**, 1048–1069 (2008). doi:[10.3390/s8021048](https://doi.org/10.3390/s8021048)
44. Gurtin, M.E., Murdoch, A.I.: A continuum theory of elastic material surfaces. *Arch. Ration. Mech. Anal.* **57**(4), 291–323 (1975)
45. Gurtin, M.E., Murdoch, A.I.: Surface stress in solids. *Int. J. Solids Struct.* **14**(6), 431–440 (1978)
46. Gheshlaghi, B., Hasheminejad, S.M.: Vibration analysis of piezoelectric nanowires with surface and small scale effects. *Curr. Appl. Phys.* **12**(4), 1096–1099 (2012)
47. Hosseini-Hashemi, S., Nahas, I., Fagher, M., Nazemnezhad, R.: Nonlinear free vibration of piezoelectric nanobeams incorporating surface effects. *Smart Mater. Struct.* **23**(3), 035012 (2014)
48. Zhang, J., Wang, C., Adhikari, S.: Surface effect on the buckling of piezoelectric nanofilms. *J. Phys. D Appl. Phys.* **45**(28), 285301 (2012)
49. Lu, P., He, L., Lee, H., Lu, C.: Thin plate theory including surface effects. *Int. J. Solids Struct.* **43**(16), 4631–4647 (2006)
50. Chen, L.-W., Lin, C.-Y., Wang, C.-C.: Dynamic stability analysis and control of a composite beam with piezoelectric layers. *Compos. Struct.* **56**, 97–109 (2002). doi:[10.1016/S0263-8223\(01\)00183-0](https://doi.org/10.1016/S0263-8223(01)00183-0)
51. Younis, M.I., Nayfeh, A.H.: A study of the nonlinear response of a resonant microbeam to an electric actuation. *Nonlinear Dyn.* **31**, 91–117 (2003). doi:[10.1023/A:1022103118330](https://doi.org/10.1023/A:1022103118330)
52. Nayfeh, A.H.: *Perturbation Methods*. Wiley, New York (1973)
53. Zhang, L.L., Liu, J.X., Fang, X.Q., Nie, G.Q.: Effects of surface piezoelectricity and nonlocal scale on wave propagation in piezoelectric nanoplates. *Eur. J. Mech. A Solids* **46**, 22–29 (2014). doi:[10.1016/j.euromechsol.2014.01.005](https://doi.org/10.1016/j.euromechsol.2014.01.005)